A Vision Based RGB Color Space

E. M. Granger*

Keywords: Color Space, RGB, Appearance, ATD, *IQ*RGB

Abstract

This paper presents a candidate standard, a wide gamut – vision based RGB color space. The candidate RGB space is operating system neutral and computationally efficient. The space has a companion uniform chromaticity space that offers an alternative to the CIELAB color space.

Introduction

The new RGB rendering space, *IQ*RGB, defined in this paper is based on the actions of the human visual system. The color space offers better arithmetic precision, color space uniformity and support for automatic white point correction. The previous ATD-RGB model is based on an expansion of the sRGB primaries. At that time it was felt this would simplify the display of the stored images. Unfortunately the AEQ (Granger 1994) primary system is not visually uniform and encompasses a very large gamut. It shares the disadvantages of the CIEXYZ space, namely, that much of the vector space is not used to render "real world" images. This requires using more bits of computational precision in XYZ just to guarantee 8-bit precision in rendered images. The solution to this problem is to employ a vision based RGB color space that is wrapped tightly around the gamut of real world colors. *IQ*RGB is designed to fit the "real world" color gamut insuring the system is 8 bit friendly.

Digital photography and scanning are becoming a dominant source of images for reproduction systems, whether it is for home or professional use. Therefore, RGB is becoming the color space of choice. The selection of the RGB primaries in the *IQ*RGB system is not arbitrary. They support a uniform appearance transform. The new transform has tristimulus values denoted ATD. The transform from *IQ*RGB to ATD is a "best" approximation to the known channels of human vision. The new model, while being linear and integer, produces a uniform chromaticity space denoted Qtd. A computationally simple model answers the need for a space that produces uniform color differences.

* Ontario Beach Systems, LLC

The ICC workflows use the CIELAB color space as the basis for transforming RGB to the colorant system used by an output device. The current practice is to convert color data to a standard CMYK. If the image data is to be rendered on a device that has nonstandard colorants, the CMYK data has to be transformed back to CIELAB. The CIELAB image must be re-transformed for reproduction on the nonstandard printer. This process has many flaws and limitations. The *IQ*RGB system is being developed and tested with known vision data. *IQ*RGB will be compared to CIE xyY and CIELAB using the same vision data.

*IQ*RGB Primaries

Opponent-process color vision theory is well known. The hue of a color can be described in terms of its redness and greenness and its yellowness and blueness. This process is called opponent because the opponents yellow-blue and red-green are not seen simultaneously. The red-green and yellow-blue responses are independent of one another. Therefore, one can never see a spectacular red-green or a beautiful yellow-blue.

The *IQ*RGB primaries are selected to produce an opponent-process based on the perceptually unique blue, green and yellow hues. The deuteranopic confusion point is used as the extraspectral red opponent. The unique blue, green and yellow hues are at wavelengths; 475, 500, and 575 nm. The extraspectral red is located at x =1.4, y = -0.4 (Wyszecki, 1982a) of the CIE xyY color space. The lines connecting the opponent hues are used as the axes of the color model. The line connecting unique red and green is the T axis and yellow and blue, the D axis. The achromatic axis is denoted A. ATD is the tristimulus equivalent of CIEXYZ. ATD can be converted to CIEXYZ by using a 3X3 matrix.

Figure 1 shows the unique yellow and blue hue locations and the D axis. Colors on the D axis are perceived as neutral by Deuteranopes. The blue primary is placed on the alychne. Points on the alychne have no luminosity. They are purely chromatic and non-luminous stimuli. Therefore, changes in the blue primary result in a change of the white point but produce no change in either the A or Y tristimulus values.

The location of the blue primary simplifies illuminant correction in digital photographs. The loci of the D illuminants over the range of color temperatures of 4,000 to 20,000 degree Kelvin are shown on Figure 1. The D illuminants lie on or close to the yellow-blue axis. Therefore, an adjustment of the blue primary's output is all that is required to change the color temperature of a reproduction.

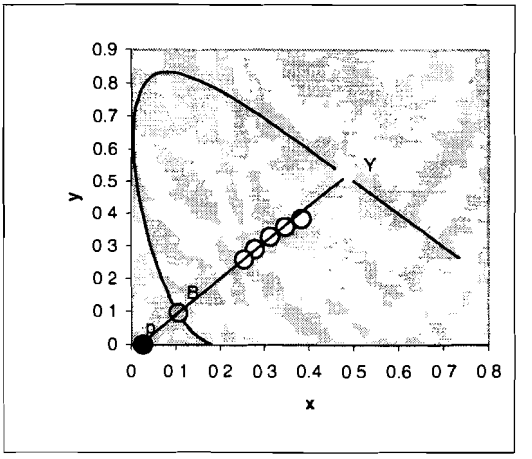

Figure 1 Blue Primary and D axis

The T axis of the ATD system lies on the line that passes thru the unique red and green hues as shown on Figure 2. Tritanopes will interpret all colors that lie on this line as neutral. Figure 3 shows both axes and the D illuminant data. This figure yields the surprising result that the axes intersect at the chromaticity coordinates of the D65 illuminant. This suggests that illuminant D65 is the natural set point for white.

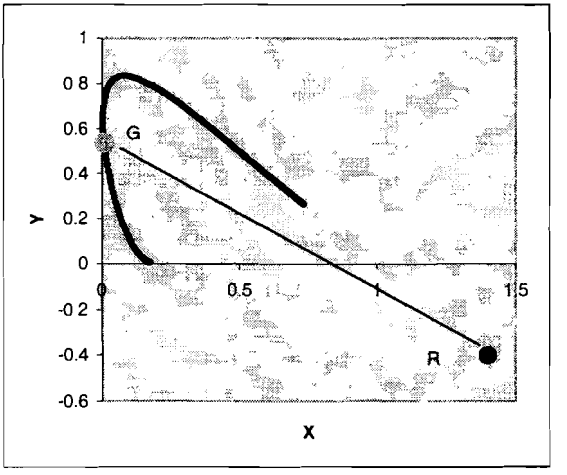

Figure 2 T axis of the ATD Color Space

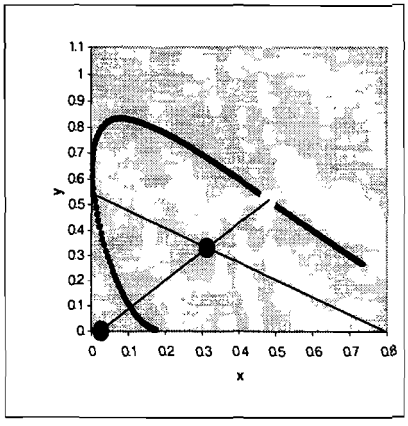

Figure 3 D65 Neutral Point

The red and green primary selection is much more complicated. These primaries must lie on a line that is parallel to the D axis. This is done to approximate the behavior of the tritanopic system. The line is also constrained to pass thru the spectrum locus at 575 nm. This is necessary to produce compact support for colors in the red-green region. The primary separation and location on the red-green line is selected so that the *IQ*RGB color space provides compact support for the most saturated colorants found in nature and industry. The gamut of these colors is called the Real World and is shown on Figure 4.

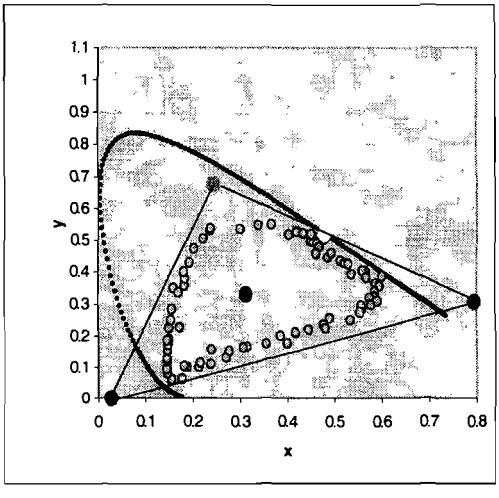

Figure 4 The Real World

The red and green primaries must be adjusted to simultaneously provide a compact support for the Real World and produce a uniform color space. In addition, the matrix relation between *IQ*RGB, CIEXYZ and the relationships and positions of the primaries are not arbitrary. ATD is created so that the luminosity function, A, of the ATD color space is proportional to Y of CIEXYZ. The resulting *IQ*RGB-ATD color space is described below.

The *IQ*RGB-ATD Color Space

The intent of the *IQ*RGB color space is to create a RGB primary set that is based on the actions of the human visual system. The chromaticity locations of the *IQ*RGB primaries are chosen so that a matrix transformation of the primaries yields a perceptually equal color space. The coefficients of the matrix must be integers, and all mathematical operations are performed in integer math. The relation between *IQ*RGB and the ATD color space is;

$$\begin{matrix} A \\ T \\ D \end{matrix} = \begin{vmatrix} 1 & 3 & 0 \\ 1 & -1 & 0 \\ 1/2 & 1/2 & -1 \end{vmatrix} * \begin{matrix} R \\ G \\ B \end{matrix} \qquad (1)$$

There is a similar but non-integer matrix between the CIEXYZ tristimulus values and those of ATD. The matrix is;

$$\begin{matrix} A \\ T \\ D \end{matrix} = \begin{vmatrix} 0.0000 & 4.0000 & 0.0000 \\ 2.5060 & -2.306 & -0.0688 \\ 0.4427 & 0.5988 & -0.9369 \end{vmatrix} * \begin{matrix} X \\ Y \\ Z \end{matrix} \qquad (2)$$

The relationships shown in Equations (1) and (2) assume a D65 white point and that (RGB) = (1,1,1) transforms to (XYZ) = (0.9501, 1.000, 1.088). The matrices given in Equations (1) and (2) define the primaries. The red primary is located at CIE (x, y), (0.7844, 0.3128), the green primary at (0.2602, 0.6650) and the blue primary at (0.0267, 0.0000).

The ATD color mixing functions, displayed on Figure 5, are computed using Equation (2). The figure shows that the mixing function for the achromatic vector, A, is scaled four (4) times that used for CIE Y. The factor of 4 is chosen to increase the precision of the integer math calculations to 10 bits and thus, eliminates the need for a compressive transformation of brightness. The diagram also shows that the transformation has kept the neutral points of the T and D vectors. The T color mixing function is zero at 475 and 575 nm where the T vector crosses the D axis. In similar fashion, The D color mixing function has no value at 500 nm where the D vector crosses the T axis.

The ATD tristimulus values are used in image manipulation to change tone scale or color balance. Rendering the image requires transforming the physical values to an appearance space. The next section of this paper discusses the development of a uniform color space. The appearance space maintains the same integer math and simple calculations, as did the definition of the ATD tristimulus values.

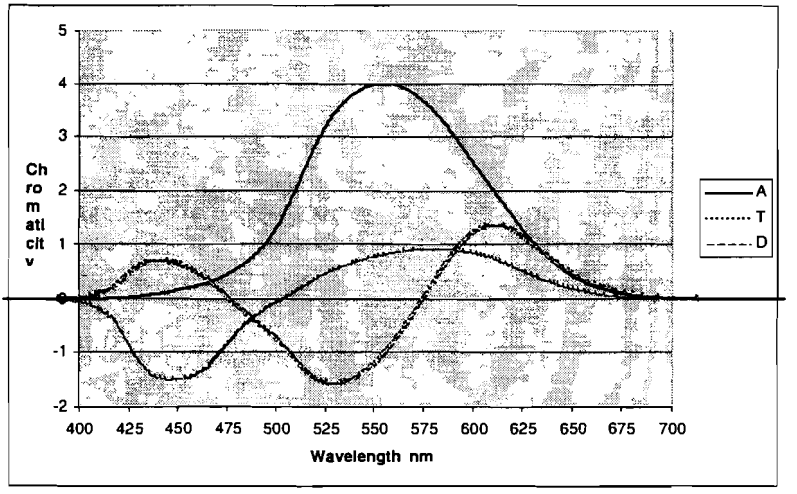

Figure 5 ATD Color Mixing Functions

The *IQ*RGB Chromaticity Diagram

Preliminary research shows that the chromatic channels' influence on the achromatic channel plays a large role in producing a uniform chromaticity space. Trial chromaticity coordinates are computed by dividing the T and D tristimulus by a normalization factor. This factor is determined by using arbitrary integer multipliers to modify the A, T and D vectors. The magnitude of the normalization factor is found to be a function of hue when the model coefficients are adjusted for best fit to large and small color difference measurements. The spectral shape of the normalization factor is similar to that of the Helmholtz-Kohlrausch, (H-K), effect (Wyszecki, 1982b).

The H-K effect or luminance additivity failure is well known. Highly chromatic colors usually appear brighter than the luminance value predicted by CIE Y. The model used in this paper assumes that the T and D channels of vision are either adding to or subtracting from the brightness of the A channel. Sanchez

and Fairchild (2001) have measured the H-K effect for very chromatic colors. They use a monitor in their experiment to produce bright and highly chromatic samples. The brightness-lightness ratios determined by their research are shown on Figure 6.

A new vector Q is defined to model the brightness evoked by the combined actions of the A, T and D channels. The Q vector is a linear function of A, T and D. The coefficients of the model for Q are constrained to be integers and are adjusted to best fit the Sanchez-Fairchild data. The equation for the Q vector is;

$$Q = A + T/2 - D \qquad (3)$$

Although the Q model is very simple, it produces a good fit to the measured H-K effect. The brightness factor, Q, is used as the normalization factor in the definition of chromaticity. Q, shown in Equation 3, produces a very reasonable uniform chromaticity space for both large and small color difference data.

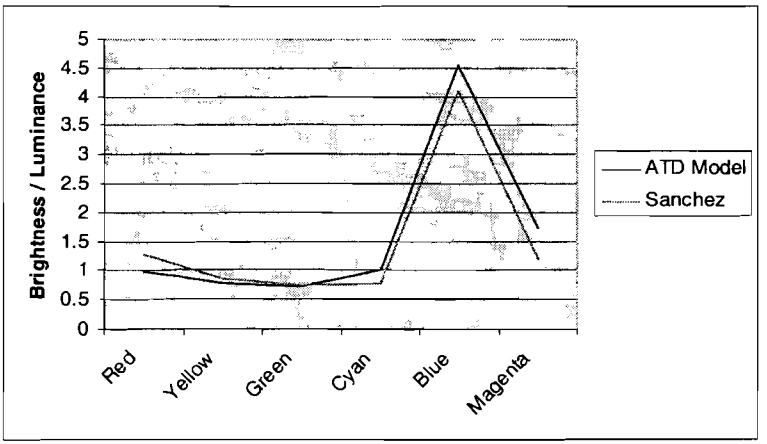

Figure 6 Brightness- Luminance Ratio

The chromaticity coordinates are defined as;

$$t = T / Q$$

and (4)

$$d = D / Q$$

The CIE 1931 spectrum locus is transformed and displayed as a function of the t and d chromaticity coordinates on Figure 7.

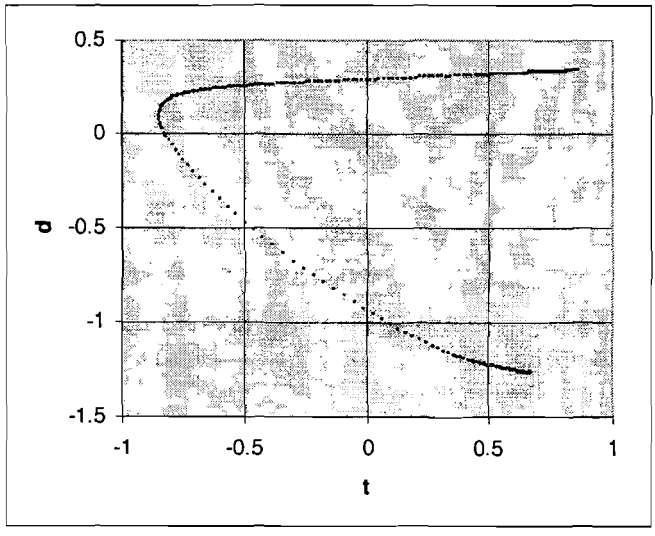

Figure 7 (t, d) Chromaticity Diagram

Testing the *IQ*RGB Model

The new RGB- ATD-Qtd model is compared with CIExyY and CIELAB to illustrate the ability of the model to predict a wide variety of vision data. All test are made at a relative luminance CIELAB L* of 50.0 and a D65 white point. The H-K effect is already modeled in the development of the chromaticity space as shown on Figure 6. The H-K effect is not modeled by either of the comparison spaces.

Wavelength Discrimination

Wavelength discrimination is a test of the uniformity of the spaces for the most saturated color, those on the spectrum locus. Figure 8 shows the wavelength discrimination data measured by Wright and Pitt (Wyszecki, 1982c).

Wavelength discrimination for *IQ*RGB and CIELAB is modeled by transforming the CIE 1931 chromaticity diagram to (t, d) and (a*, b*) and taking the inverse of the distance between adjacent 1 nm points on the spectrum locus as shown on Figure 7. The just noticeable difference (JND) between points is scaled to match the known visual data. The Qtd wavelength JND versus wavelength is shown on Figure 9 and the *IQ*RGB JNDs are displayed on

Figure 10. The comparison of the curves on these three plots shows that *IQ*RGB transformation best models the known wavelength data.

Large Color Differences

The uniform color scales of the OSA Color Systems (Wyszecki, 1982d) are used to test the uniformity of the *IQ*RGB model as compared to the CIE xyY and CIELAB color spaces. The comparisons are all made at a CIELAB-L* of 50.0. Figure 11 displays the CIExyY data determined by the OSA committee. Also shown on Figure 11 is the *IQ*RGB transformation of the CIE xyY data along with the CIELAB transformation. In comparison, the *IQ*RGB model appears to produce a more uniform spacing of data points than does CIELAB.

The Munsell Renotation System (Wyszecki, 1982e) is another well-researched uniform color scale. Figure 12 plots the CIE xyY data at the level where CIE-L* = 50.0. This data is corrected to a D65 white point. This is necessary since the *IQ*RGB color system assumes a D65 white. The figure displays the *IQ*RGB transformed Munsell data. In like manner, Figure 12 shows the D65 normalized Munsell data transformed to CIELAB. Again, the *IQ*RGB model generates uniform data point spacing. The CIELAB transformation produces exaggerated saturation spacing for the yellow region. The hue angle spacing appears to be less even with a large gap in the green region. The CIELAB lines of constant hue have much more curvature than those of *IQ*RGB.

Small Color Differences

MacAdam's (Wyszecki, 1982f) color matching ellipse experiment is well known. This paper uses his data as a further test of the *IQ*RGB model. One problem with this data is that other experimenters, including MacAdam, have not been able to repeat his original experiment. Many factors such as acuity, age, and observer metamerism influence the discrimination task. All of these effects lead to large variations in the orientation, eccentricity and size of the ellipses. This paper includes the color matching ellipse data of MacAdam and Wyszecki-Fielder (observer G.F.)(Wyszecki, 1982g). Since there is large variance among observers both sets of data are included to test of the *IQ*RGB model. Figure 12 shows the comparison of the Wyszecki-Fielder and CIELAB transformations of the MacAdam ellipse data and Figure 13, the Wyszecki-Fielder ellipse data. The *IQ*RGB transformation produces more uniform ellipses than CIELAB for both test samples. The *IQ*RGB transformation was not tuned for the color matching ellipse data. The *IQ*RGB model has to pass all the test comparisons. As shown in the sections above, the *IQ*RGB model performs well for the entire set of tests.

Conclusions

*IQ*RGB, the companion ATD luminance- chromanance color space and the Qtd appearance space have been tested against a wide variety of visual data and are found to produce a reasonable uniform color space for application in the graphic arts. This paper has introduced the concept of the Real World of colors that encompasses all of the surface colors in nature and industry. The *IQ*RGB color space is introduced as an efficient vector set that is a compact support for the Real World. The *IQ*RGB vectors are chosen so that a simple binary integer transformation of the vectors produces a reasonably uniform color space. The ATD-Qtd color space is developed for efficient communication of color data. As such, the model is not meant to be comprehensive and is limited to the narrow range of communicating data in digital imaging.

Acknowledgment

The author thanks Michael Sanchez and Mark Fairchild for many helpful discussions on the H-K effect. Their data is essential to the final definition of the *IQ*RGB- ATD model.

Literature Cited

Granger, E.M.

1994 " ATD, Appearance Equivalence, and Desktop Publishing", SPIE, Vol. 2170

Sanchez, M and Fairchild, M

2001 " Perceptual Amplification of Color: Observer Data and Models," CIC9, Ninth Color Conference, Scottsdale, AZ

Wyszecki, G. and Stiles, W.S.

1982a "Color Science: Concepts and Methods, Quantitative Data and Formulae" (Wiley, New York), 2nd ed, 615 pp.

1982b, 410 pp.

1982c, 570 pp.

1982d, 871 pp.

1982e, 840 pp.

1982f, 309 pp.

1982g, 801 pp.

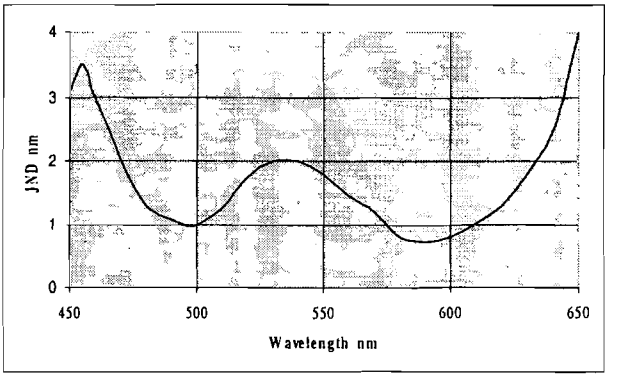

Figure 8 Wavelength Discrimination -Wright & Pitt

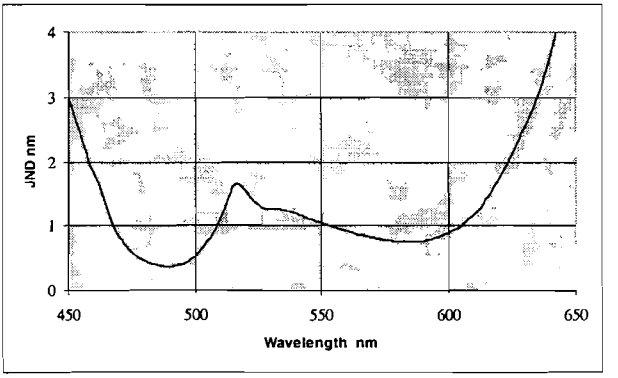

Figure 9 Wavelength Discrimination -*IQ*RGB

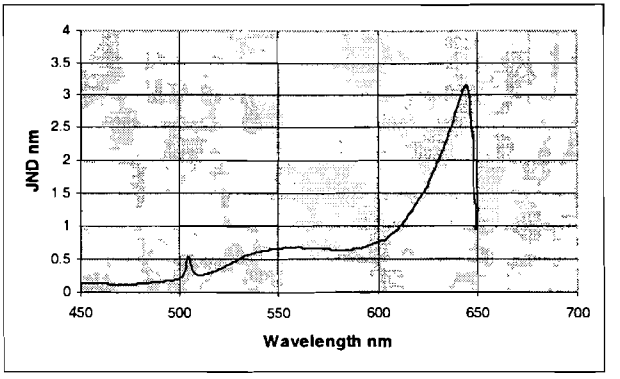

Figure 10 Wavelength Discrimination -*CIELAB*

CIExyY

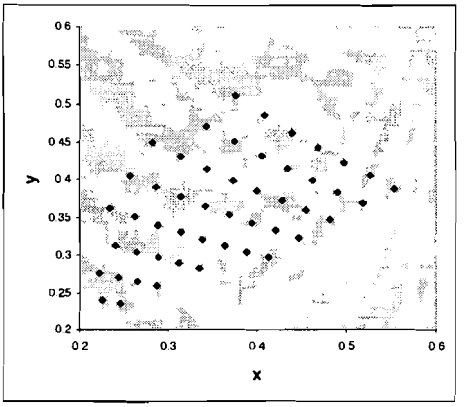

*IQ*RGB

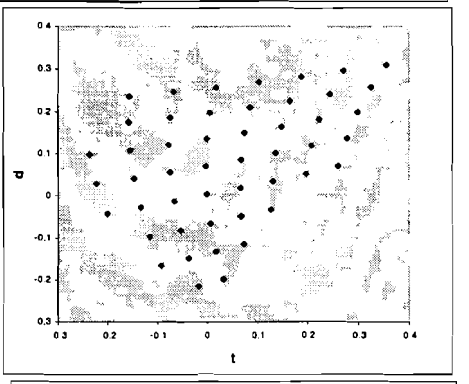

CIELAB

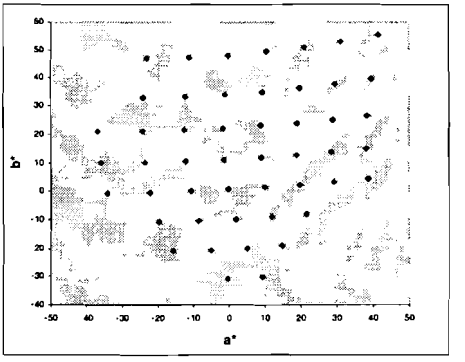

Figure 11 OSA Color System

CIExyY

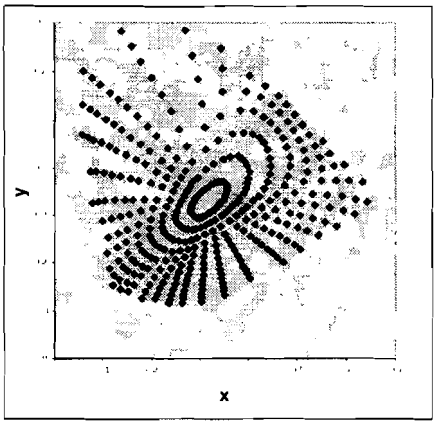

*IQ*RGB

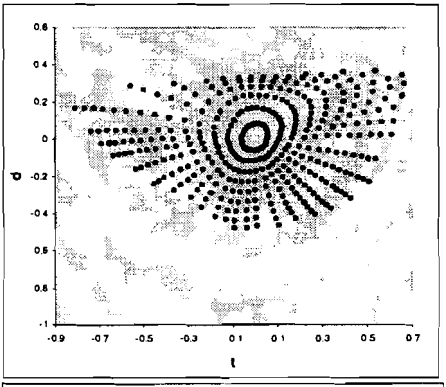

CIELAB

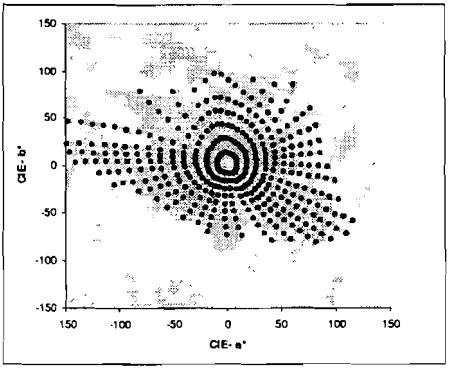

Figure 12 Munsell Renotation System

CIExyY

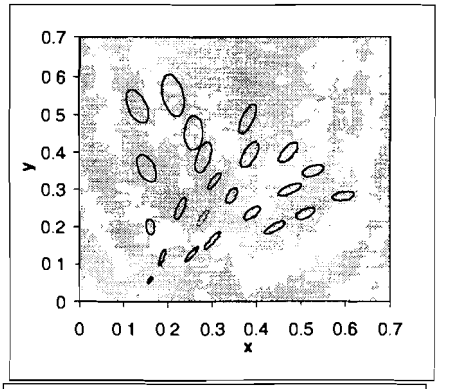

*IQ*RGB

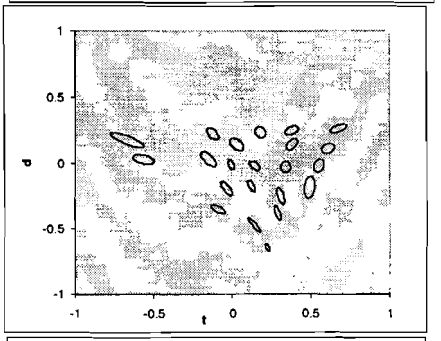

CIELAB

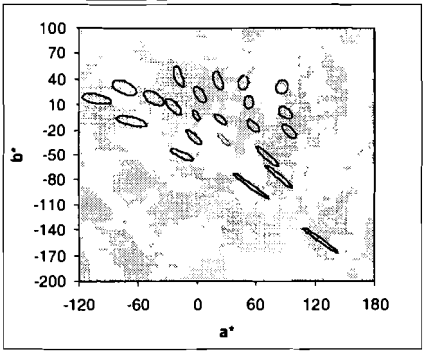

Figure 13 MacAdam Color Matching Ellipses

CIExyY

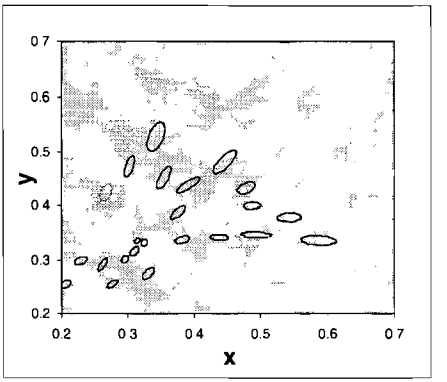

*IQ*RGB

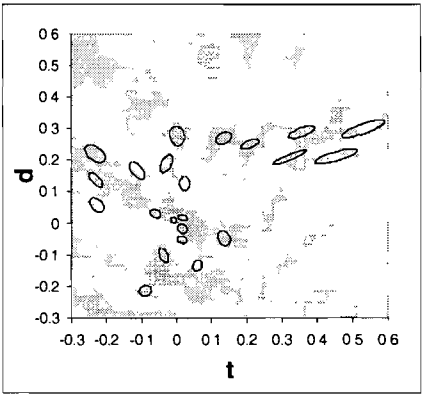

CIELAB

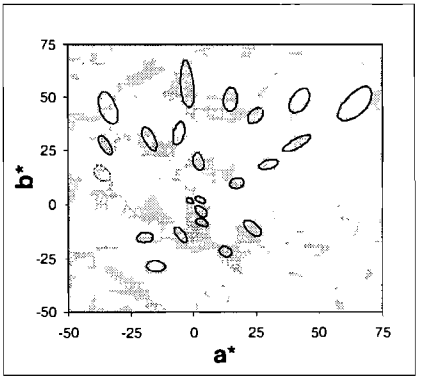

Figure 14 Wyszecki-Fielder Color Matching Ellipses